Activation of HIF-1α (hypoxia inducible factor-1α) prevents dry eye-induced acinar cell death in the lacrimal gland

Y Seo[1], YW Ji[1], SM Lee[2,3], J Shim[1], H Noh[1], A Yeo[1], C Park[4], MS Park[4], EJ Chang[5] and HK Lee*[,1,6]

The pathogenesis of immune-mediated lacrimal gland (LG) dysfunction in Sjögren's syndrome has been thoroughly studied. However, the majority of dry eye (DE) is not related to Sjögren type, and its pathophysiology remains unclear. The purpose of this study was to determine and investigate the protective mechanisms against DE stress in mice. DE induced prominent blood vessel loss without apoptosis or necrosis in the LG. Autophagic vacuoles, distressed mitochondria, and stressed endoplasmic reticulum were observed via electron microscopy. Immunoblotting confirmed the increase in autophagic markers. Glycolytic activities were enhanced with increasing levels of succinate and malate that, in turn, activated hypoxia-inducible factor (HIF)-1α. Interestingly, the areas of stable HIF-1α expression overlapped with COX-2 and MMP-9 upregulation in LGs of DE-induced mice. We generated HIF-1α conditional knockout (CKO) mice in which HIF-1α expression was lost in the LG. Surprisingly, normal LG polarities and morphologies were completely lost with DE induction, and tremendous acinar cell apoptosis was observed. Similar to Sjögren's syndrome, CD3$^+$ and CD11b$^+$ cells infiltrated HIF-1α CKO LGs. Our results show that DE induced the expression of HIF-1α that activated autophagy signals to prevent further acinar cell damage and to maintain normal LG function.

Dry eye (DE) disease afflicts >15% of the urban population.[1,2] It is characterized by discomfort, visual disturbance, and tear film instability with potential damage to the ocular surface because of increases in tear film osmolarity and inflammation. Therefore, it substantially affects the quality of life.[3,4] The lacrimal gland (LG), ocular surface, and their interconnecting neural reflex loops work together to produce tears that prevent ocular surface damage from external stimuli. This is defined as the lacrimal functional unit.[5,6]

LGs can become the target of the immune system and show signs of inflammation that impair its normal function. A progressive loss of exocrine gland function because of glandular damage is induced by lymphocytic infiltration into these target organs. In Sjögren's syndrome, CD4$^+$ T cells infiltrate into accompanying B cells.[7–9] Various studies have been conducted on the immune-mediated pathogenesis in LGs of patients with Sjögren's syndrome. However, most of the DE incidences are non-Sjögren's syndrome in which

nonimmunological injuries that are related to glandular dysfunction are observed.[8] LG changes and damages in non-Sjögren's syndrome are less elucidated than those in Sjögren's syndrome. In Sjögren's DE disease, the secretory impairment of lacrimal and salivary glands may be related to the extent of lymphocytic infiltration and loss of glandular tissue. However, in non-Sjogren's disease, inflammatory cell invasion and lymphocytic infiltration are reduced, and other factors may contribute to the impairment in secretory function.[8,10,11]

LGs are highly vascularized tissues that secrete water and ions that are transported across the glandular epithelium. Vascular integrity and blood flow are essential for the normal physiological function of LGs. The effects of DE on these factors are not well characterized. The mechanisms by which LG acinar cells protect their secretory function and polarity against DE are also unknown. Recently, we found that prostaglandin (PG) E$_2$ and cyclooxygenase-2 (COX-2) levels

[1]Institute of Vision Research, Department of Ophthalmology, Yonsei University College of Medicine, Seoul, Korea; [2]Schephens Eye Research Institute, Harvard Medical School, Boston, MA, USA; [3]Department of Ophthalmology, Hallym University Sacred Heart Hospital, Hallym University College of Medicine, Gyeonggi-do, Korea; [4]Clinical Trials Center, Yonsei University College of Medicine, Seodaemun-gu, Seoul, Korea; [5]Department of Anatomy and Cell Biology, University of Ulsan College of Medicine, Seoul, Korea and [6]Institute of Corneal Dystrophy Research, Yonsei University College of Medicine, Seodaemun-gu, Seoul, Korea
*Corresponding author: HK Lee, Department of Ophthalmology, Severance Hospital, Institute of Vision Research, 211 Eonju-ro, Gangnam-gu, Seoul 135-720, Korea. Tel: + 82 2 2019 3444; Fax: + 82 2 3463 1049; E-mail: hyungkeun.lee@gmail.com

Abbreviations: DE, dry eye; LG, lacrimal gland; PGE, prostaglandin E; COX-2, cyclooxygenase-2; PG, prostaglandin; HIF-1α, hypoxia-inducible factor-1α; CKO, conditional knockout; BV, blood vessel; LV, lymphatic vessel; LYVE, lymphatic vascular endothelial gene; qPCR, quantitative PCR; PECAM, platelet endothelial cell adhesion molecule; TUNEL, terminal deoxynucleotidyl transferase-mediated dUTP nick end labeling; ER, endoplasmic reticulum; LC3, light chain 3; CHOP, C/EBP homolog protein; eIF-2α, eukaryotic translation initiation factor-2α; p-PERK, phosphorylated protein kinase-like ER kinase; BNIP3, Bcl2/adenovirus E1B-interacting protein 3; ATG6, autophagy-related gene 6; AMPK, AMP-activated protein kinase; LC-MS, liquid chromatography-mass spectrometry; GABA, γ-aminobutyric acid; VEGF, vascular endothelial growth factor; LDH, lactate dehydrogenase; EPO, erythropoietin; DAMP, damage-associated molecular pattern; MMP, matrix metalloproteinase; TNF, tumor necrosis factor; IL, interleukin; WT, wild type; AAD, aminoactinomycin D; mTOR, mammalian target of rapamycin; GPR, G protein-coupled receptor

are significantly increased in LGs of humans and mice with DE.[12] However, the mechanisms by which PG synthesis is increased and the exact roles of these PGs in the pathophysiology of DE require further elucidation.

The purpose of this study was to investigate the natural protective mechanisms of LGs against DE stress in mice. In addition, we developed a novel hypoxia inducible factor (HIF)-1α conditional knockout (CKO) model to determine the role of HIF-1α in the morphological changes in acinar cells and vascular integrity in DE-induced LGs.

Results

DE-induced pathological changes in mouse LGs *in vivo*.

To investigate the effects of DE on the pathology of LG, mice were kept in a controlled environmental chamber for 4 weeks, and then killed. After 10 days of DE induction, LG size, which was measured by calculating the maximum length, was significantly decreased from 5.2 ± 0.9 to 3.9 ± 1.1 mm (Figure 1a). Interestingly, the LGs became pale and white after DE induction in a time-dependent manner. This may reflect reduced vascularity
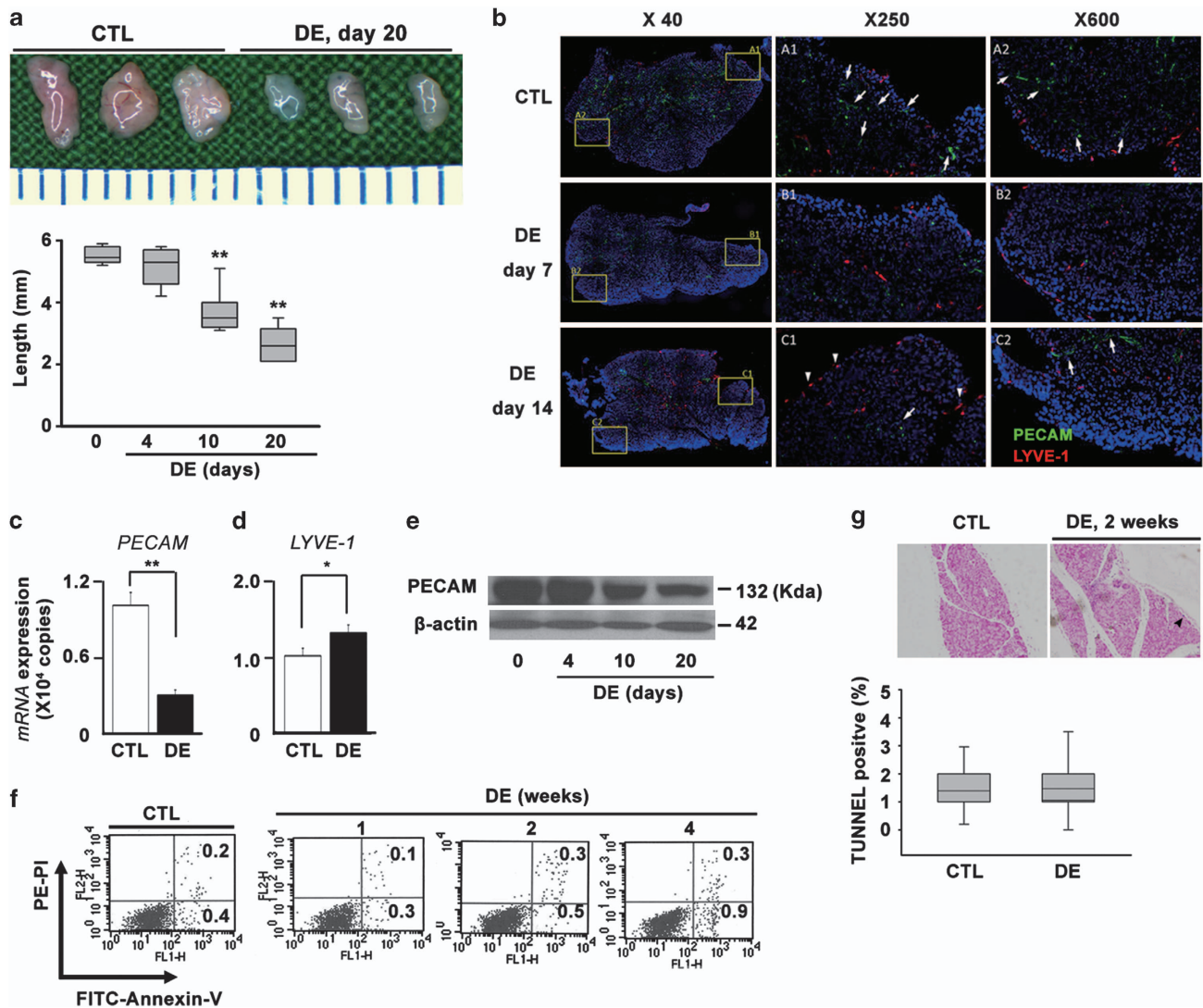

Figure 1 Dry eye (DE)-induced pathological changes in the mouse lacrimal gland (LG). (**a**) Determination of the size of LGs of DE-induced mice. Extraorbital LGs from five mice were secured after DE induction. The maximum LG lengths were measured at each time point (**$P < 0.01$, one-way ANOVA). (**b**) Immunofluorescence staining for blood vessels (PECAM, green) and lymphatics (LYVE-1, orange). Confocal microscopic images from the entire section of slides were automatically stitched into whole images (upper row: non-DE-induced control, middle row: 7 days after DE induction, lower row: 14 days after DE induction (arrows: PECAM-stained blood vessels, arrowhead: LYVE-1-stained lymphatics, blue: DAPI-stained nuclei)). (**c** and **d**) The qPCR analysis for PECAM and LYVE-1 in DE-induced LGs. LGs were secured after 1 week of DE induction, and RT-PCR was performed using primers specific for PECAM-1 and LYVE-1 (*$P < 0.05$, **$P < 0.01$, Student's *t*-test). (**e**) Immunoblotting for PECAM expression in DE-induced LGs. After DE induction, LGs were secured and immersed in 0.1 ml RIPA buffer with the protease inhibitor cocktail. Anti-PECAM (1 : 2000) and anti-β actin (1 : 4000) were used. Each condition included six LGs. (**f**) LGs from each condition of DE induction were collected and incubated with 0.1 μg/ml collagenase with 0.1% hyaluronidase solution for 2 h at 37 °C. Then, LGs were minced and sieved to yield single-cell suspensions. The cells were incubated with anti-annexin V (1 : 100) and anti-PI (1 : 100) for 1 h. Analysis was performed by FACSCaliber (BD Biosciences). (**g**) LG tissues that were fixed with 4% paraformaldehyde were stained using the Boehringer Mannheim TUNEL kit and counterstained with hematoxylin

(Figure 1a and Supplementary 1). Next, we assessed the effects of DE on the pathology of blood vessels (BVs) and lymphatic vessels (LVs) in LGs. The number of CD31-expressing BVs (green) was significantly decreased, starting at 1 week after induction (Figure 1b, middle and lower rows). Under normal conditions, BVs were equally detected in the central and peripheral areas of LGs (Figure 1b, upper row white arrows). At 2 weeks of DE induction, BV loss was greater in the peripheral area compared with that of 1 week after induction (Figure 1b and Supplementary 2). Many LVs were found on the surface of LGs under normal and DE-induced conditions, although DE did not affect the number of LVs. Moreover, lymphatic vascular endothelial gene (LYVE)-1-expressing structures were upregulated in DE-induced LG. The changes in the expression levels of BVs and LVs by DE were confirmed using quantitative PCR (qPCR; Figures 1c and d). Similarly, the protein expression of platelet endothelial cell adhesion molecule (PECAM) was significantly decreased by DE stress (Figure 1e).

Because DE reduced the volume of LGs and diminished vascularity, apoptotic cell death was assessed. DE induction did not increase the number of Annexin-V$^+$ apoptotic cells (Figure 1f), and the number of TUNEL (terminal deoxynucleotidyl transferase-mediated dUTP nick end labeling)-positive cells remained low (Figure 1g).

Enhanced endoplasmic reticulum (ER) stress and autophagy activation in LGs of DE-induced mice. Using the transmission electron microscope, severe intracellular

organelle derangement was found in LGs of DE-induced mice (Figure 2A). Compared with normal LGs (Figures 2Aa and b), vacant vacuoles (Figure 2Ac), dilatation of the ER (Figure 2Ad, blue arrow), decreased number of mitochondria with loss of cristae structures (Figures 2Ad, h), vacuolation, and autophagosomes were characteristically found in DE-induced LGs (Figures 2Ae, f and g). Some DE-induced acinar cells exhibited increased numbers of secretory vesicles, whereas other cells showed severely decreased number of vesicles (Figures 2Ae and g). Autophagosomes containing dead acinar cells were engulfed by macrophages (M, Figure 2Af). Numerous vacuolization is a characteristic of autophagy,[13] and microtubule-associated protein 1A/1B-light chain 3 (LC3) expression was significantly increased by DE induction (Figure 2B and Supplementary 3). In addition, the levels of C/EBP homolog protein (CHOP; ER stress-related protein), eukaryotic translation initiation factor (eIF)-2α, phosphorylated protein kinase-like ER kinase (p-PERK), Bcl2/adenovirus E1B-interacting protein 3 (BNIP3), and Beclin 1/autophagy-related gene 6 (ATG6) were significantly increased (Figure 2C and Supplementary 3). The phosphorylation and expression of 5′ AMP-activated protein kinase (AMPK) were unchanged in LGs until the 3-week time point (Figure 2D).

HIF-1α activation and glycolytic conditions in LGs of DE-induced mice. Our results demonstrate that DE decreased BVs, disrupted intracellular organelles, and increased autophagy in LGs. In addition, the concentrations
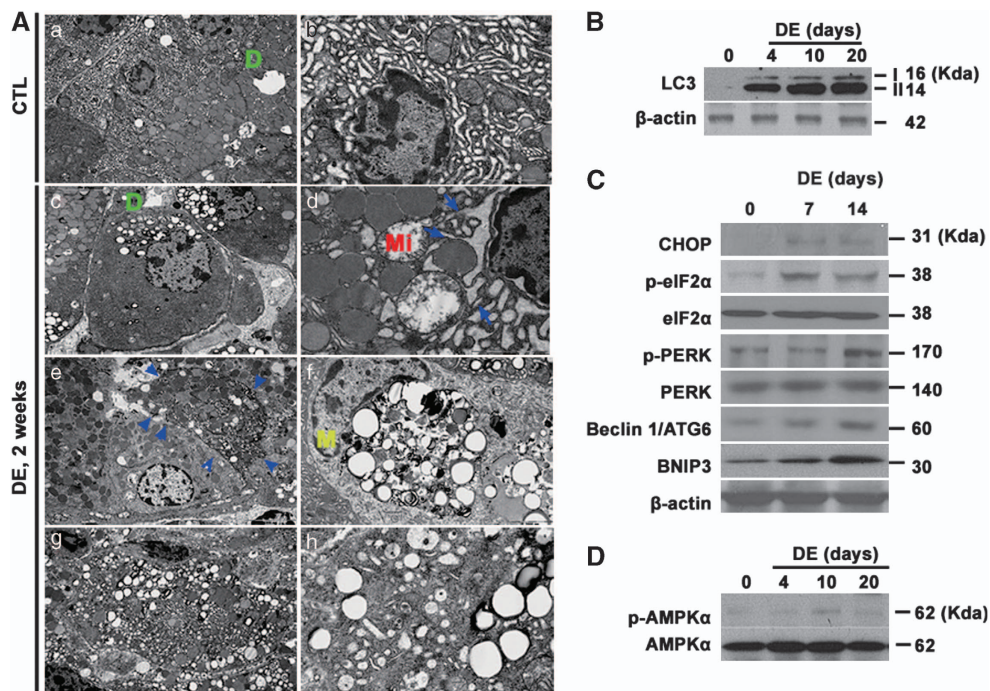

Figure 2 Determination of ER stress status and morphological intracellular organelle changes in DE-induced LGs. (**A**) Non-DE-conditioned control LGs (CTL) are depicted in the upper row. (a and b) Secretory vesicles that oriented to secretory ductules (D) with well-developed ER were found. (c and d) At 1 week after DE induction, increased electron density in the cytoplasm, vacuolization (V), loss of mitochondrial cristae (Mi), and marked dilatation of ER (blue arrow) were found. (e) Dead cells that paced with disorganized organelles (blue arrowhead) and (f) engulfing cell debris by macrophages (M) were also detected. (g) Vacuolization with autophagosomes and (h) the loss of orientation of intracellular organelles were noted. (**B**–**D**) Immunoblotting for LC3 and ER stress markers were performed in DE-induced LGs. All the immunoblot experiments were repeated three times

of lactate and alanine, which are markers for glycolysis, were significantly increased with DE stress (Figures 3a and b). The concentration of lactate in DE-induced LGs was 25.6 times higher than normal at 1 week of induction. The concentrations of glycolysis and Krebs cycle intermediates were also measured using liquid chromatography-mass spectrometry (LC-MS). The concentrations of succinate, γ-aminobutyric acid (GABA), and citrate were significantly elevated by DE induction in a time-dependent manner. In contrast, isocitrate and glutamate concentrations were drastically decreased (Figure 3c and Supplementary 4).

HIF-1α is a key transcription factor that rapidly adapts to reductions in oxygen levels, thus triggering autophagy.[14,15] The expression of HIF-1α peaked after 1 week of DE induction (Figure 3d). After 2 weeks of induction, HIF-1α levels slightly decreased. However, the expression level of HIF-1α was still significantly higher than that of the non-DE control. DE also upregulated the downstream signaling factors of HIF-1α, such

as vascular endothelial growth factor (VEGF), lactate dehydrogenase (LDH), and erythropoietin (EPO) (Figure 3e). Under normal conditions, HIF-1α staining was detected in some BVs (Figure 3f, left column, red arrow). With DE induction, HIF-1α staining was patch-like and enhanced in the acinar cells, especially in the peripheral areas (Figure 3f, middle, black arrow), and it was not detected in infiltrated cells (Figure 3f, right column, green arrow) and ductal areas. Because succinate and fumarate are damage-associated molecular pattern (DAMP) signals in various conditions,[16] we determined whether these glucose metabolites enhanced HIF-1α expression. Indeed, HIF-1α expression was significantly enhanced by treatments with a 20 μM solution containing succinate, GABA, or lactate (Figure 3g).

Relationship between HIF-1α and COX-2 in LGs of DE-induced mice. COX-2 levels were increased in the LGs of DE mice.[12] COX-2 and HIF-1α are known to be
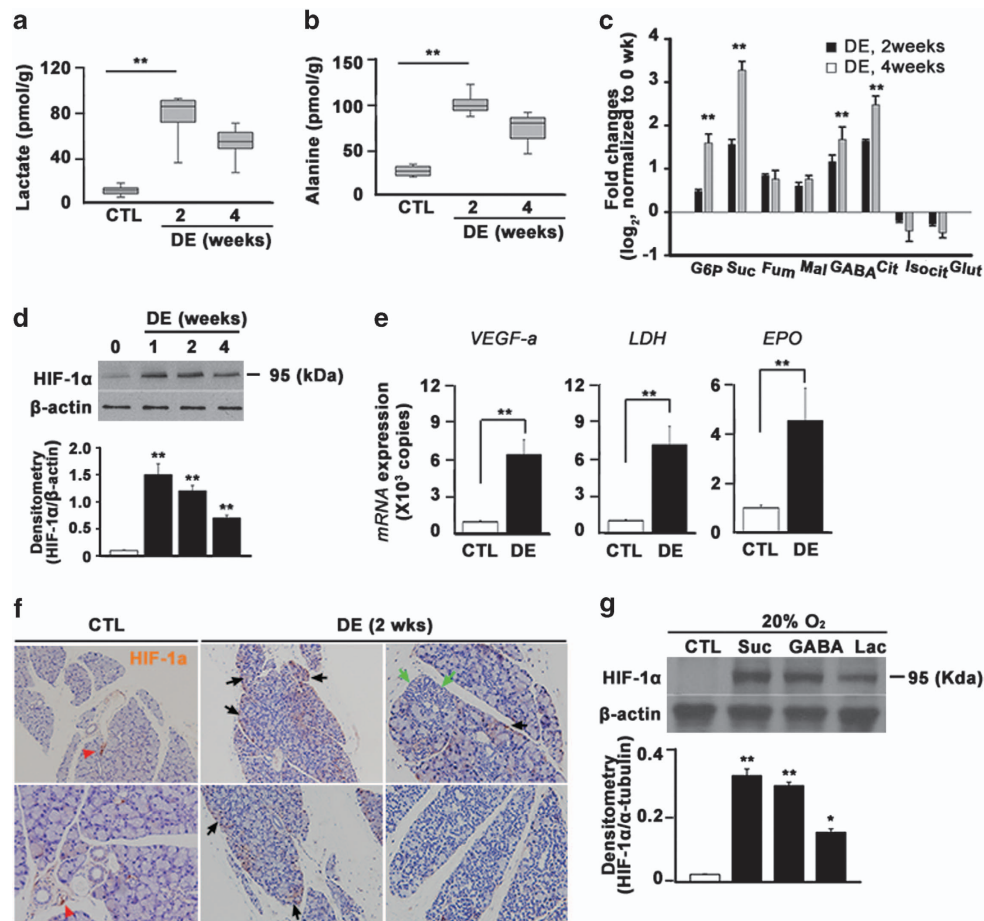

Figure 3 Oxidative stress and hypoxia-inducible factor-1α (HIF-1α) induction in DE-induced LGs. (**a–c**) Concentrations of lactate, alanine, and other glycolytic metabolites were measured in LGs from control (CTL, $n = 4$) and DE-induced mice ($n = 6$ at each time point). All metabolites were measured by hydrophilic interaction liquid chromatography (HILIC). GABA and succinates levels were measured using SeQuant ZIC-HILIC (Umea, Sweden). Detailed experimental details are described in the Materials and Methods section (**$P < 0.01$; G6P, glucose 6 phosphate; Suc, succinate; Fum, fumarate; Mal, malate; GABA, γ-aminobutyric acid; Cit, citrate; Isocit, isocitrate; Glut, glutamate) (**d**) Immunoblot for HIF-1α was performed with DE-induced LGs (**$P < 0.01$, one-way ANOVA). (**e**) VEGF-a, lactate dehydrogenase (LDH), and erythropoietin (EPO) levels were measured in LGs from CTL and DE-induced mice (2 weeks) via qPCR (**$P < 0.01$, Student's *t*-test). (**f**) Immunohistochemical staining for HIF-1α expression was performed in LGs from CTL and DE-induced mice. The red arrowhead indicates HIF-1α-stained blood vessels (left upper) and the glandular epithelium (left lower) with leukocyte infiltration (green arrows). The black arrow indicates HIF-1α staining enhanced in the acinar cells in the peripheral areas. (**g**) HIF-1α expression in the presence of glycolytic metabolites was determined using LG organ culture. Fresh LGs were immersed in organ culture medium for 6 h. Afterwards, serum-free organ culture medium with a 20 μM solution containing succinate (suc), GABA, or lactate (Lac) was added for 12 h. Then, HIF-1α expression was detected via immunoblotting (*$P < 0.05$, **$P < 0.01$, one-way ANOVA)

interregulated in various pathological conditions, including inflammation, carcinogenesis, apoptosis, and hypoxia.[17–19] Therefore, the effect of HIF-1α on COX-2 levels in the LGs of DE-induced mice was determined.

DE increased COX-2, but not COX-1, levels in LGs. COX-2 levels remained elevated until the 4-week time point (Figures 4a and b). To define the increase in COX-2 expression in LGs, CD45^{+} bone marrow-derived cells were separated from CD45^{–} cells by FACS Aria III Cell Sorter (BD Biosciences, San Jose, CA, USA). After DE induction, enhanced COX-2 levels were found only in CD45^{–} cells (Figure 4c). This suggests that COX-2 is upregulated only in acinar cells. Interestingly, immunostaining results revealed that COX-2 and HIF-1α expression was detected mainly in peripheral lacrimal glandular cells, but not in the central or inflammatory cell-infiltrated areas (Figure 4d). Moreover, most of the COX-2-expressing areas overlapped with HIF-1α-expressing areas (arrow and arrowhead in Figure 4d). Increased matrix

metalloproteinase 2 (MMP2) and MMP9 levels were also observed in these overlapping areas (Supplementary 5).

To determine the levels of COX-2-related inflammatory cytokines in LGs, DE-induced mice were subcutaneously injected with celecoxib, a COX-2 specific inhibitor (20 μM, 0.1 ml, b.i.d.). Interleukin (IL)-1β, tumor necrosis factor-α (TNF-α), IL-6, and IL-8 mRNA levels were significantly decreased in celecoxib-treated, DE-induced LGs (Figure 4e). The protein levels of IL-1β and TNF-α, which are both upregulated upon HIF-1α activation, were slightly increased after 1 and 2 weeks of DE induction (Figures 4f and g). Compared with IL-1β, TNF-α levels were more significantly enhanced and remained elevated until 4 weeks of DE induction (Figure 4g).

Role of HIF-1α in cell death and autophagy in the LGs of DE-induced mice. The role of HIF-1α in DE-induced cell death and autophagy was investigated using the HIF-1α CKO
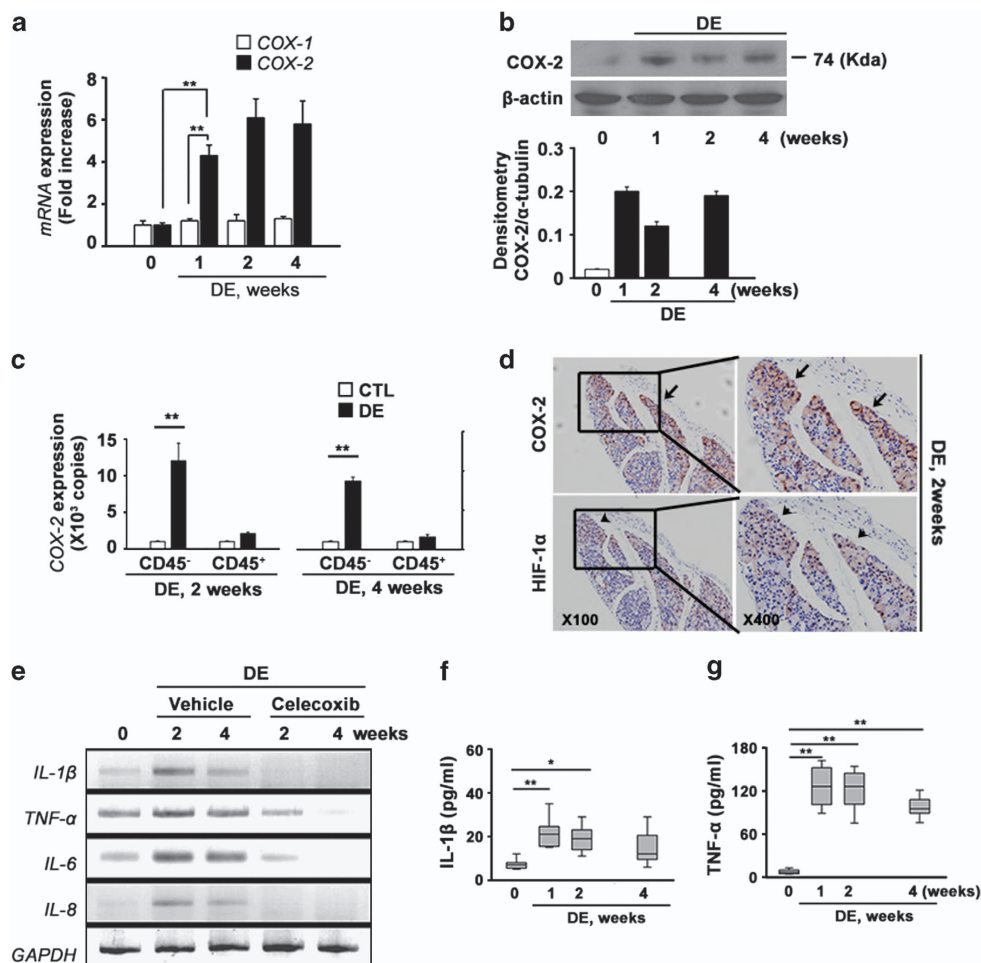

Figure 4 Expression of COX-2 and its relationship with HIF-1α in LGs from DE-induced mice. (**a**) The mRNA expression of cyclooxygenase (COX)-1 and COX-2 in LGs was determined by qPCR (**P < 0.01, Student's *t*-test). (**b**) COX-2 immunoblotting was performed in LGs from DE-induced mice at different time points. All experiments were performed at least three times and the representative blots are shown. (**c**) CD45^{+} and CD45^{–} cells were separated from DE-induced LGs by FACS Aria (BD Biosciences). mRNA was extracted from CD45^{+} and CD45^{–} cells, respectively. Then, COX-2 mRNA levels were determined by qPCR (**P < 0.01, Student's *t*-test). Three independent experiments with more than 10 LGs in each were conducted. (**d**) COX-2 and HIF-1α expression patterns were determined by immunohistochemical staining. Left column: × 100 magnification, right column: × 400 magnification. Arrows indicate COX-2-positive areas, and arrowheads indicate HIF-1α-positive areas. (**e**) At 1 week after DE induction, celecoxib (0.05%) or its vehicle was topically administered for 2 and 4 weeks. LGs were then secured, and PCR was performed for IL-1β, TNF-α, IL-6, IL-8, and GAPDH. (**f** and **g**) ELISAs were used to detect IL-1β (**f**) and TNF-α (**g**) levels in LGs (*P < 0.05, **P < 0.01, one-way ANOVA)

model. Before DE induction, the size and weight of LGs from wild-type (WT; B6), floxed, and HIF-1α CKO mice were not significantly different (Figure 5a). However, the size and weight of LGs from HIF-1α CKO mice were drastically decreased after 1 week of DE induction, and this continued until the 2-week time point.

DE caused shrinking of cytoplasms with the widening of interlobular spaces in LG acinar cells of WT mice. Pyknotic nuclei were not found (Figure 5b, left column). Before DE induction, HIF-1α CKO LGs were not morphologically different from WT LGs (Figure 5b, middle column). However, after 10 days of DE induction, the majority of the normal secretory structure had collapsed. The secretory ducts were significantly dilated (blue arrows) and were filled with eosinophilic materials, and few acinar tissues were found (Figure 5b, right column). Moreover, remaining acinar tissues lost their polarity and were replaced by ductal structures. Pyknotic condensation of the nucleus was observed, and the cytoplasm was significantly decreased. LG structure and polarity were more severely damaged in the peripheral area that was completely replaced with a few collagenous matrix-containing cells.

To determine the mechanisms by which DE caused significant and early changes in LGs of HIF-1α CKO mice, acinar cell apoptosis was assessed. Marked increases in apoptotic cells ($7AAD^-AnnexinV^+$) were found in HIF-1α CKO LGs compared with floxed or WT LGs (Figure 5c). After 2 weeks of DE induction, Annexin V^+ cells were increased to 50.7% in LGs (Figure 5c). WT or floxed LGs contained $<0.1\%$ Annexin V^+ cells. Moreover, $7\text{-}AAD^+$ cells were increased in HIF-1α CKO LGs. The apoptotic marker, Bax, and the anti-apoptotic marker, Bcl-xL, were significantly increased and decreased, respectively, in HIF-1α CKO LGs at 1 week of induction (Figure 5d). Decreasing Beclin 1 and increasing caspase 3 levels were also observed in these LGs (Figure 5d). In addition, compared with WT LGs, PECAM expression was significantly downregulated by DE induction in HIF-1α CKO LGs (Figure 5e).

As previously reported,[12] COX-2 levels were significantly increased in LGs of DE-induced WT mice. Interestingly, COX-2 was not detected in LGs of DE-induced HIF-1α CKO mice (Figure 5f). FACS analysis results showed that significant numbers of inflammatory cells were infiltrated in HIF-1α CKO LGs than in WT. After 2 weeks of DE induction, 0.3% and 9.5% of cells in the LGs of WT and HIF-1α CKO mice, respectively, were $CD3^+$ (Figure 5g). In addition, 6.4% and 13.8% of cells in WT and HIF-1α CKO LGs, respectively, were $CD11b^+$ ($P<0.001$). Levels of IFN-γ, IL-1β, and TNF-α were significantly upregulated in HIF-1α CKO LGs than in WT LGs at 2 weeks of DE induction (Figure 5h). Furthermore, TNF-α level were 50 times higher in HIF-1α CKO LGs.

Discussion

The novel findings of the present work are the following: (1) DE decreased and increased the numbers of BVs and LVs, respectively, in LGs at the early time points, and this eventually led to hypoxia; (2) DE induced metabolomic changes in LGs, including increased glycolytic activities, autophagosomes, intracytoplasmic vacuolization, and disruptions of mitochondrial cristae; (3) HIF-1α was an important transcriptional regulator in DE stress-conditioned LGs and prevented acinar cell death, and HIF-1α CKO LGs exhibited significantly increased acinar cell apoptosis and the loss of glandular structures and polarities; and (4) the blockage of HIF-1α-COX-2 axis enhanced inflammation in LGs by elevating cytokine expression and inflammatory cell infiltration.

DE has been recognized as a disturbance of 'lacrimal functional unit', an integrated system comprising LGs, ocular surface, and sensory motor nerves that connect them.[6] If any portion of this functional unit is compromised, lacrimal gland support to the ocular surface is impeded. However, as the majority of DE researches have focused on the ocular surface damage and its recovery by topical treatments, cellular and molecular mechanisms responsible for impairing LG secretion and neural derangements are still poorly understood and require further investigation in the future.[9] This study proved that the pathophysiologic changes in DE induced stress and natural protective mechanisms, in terms of LG vascularities.

Activation of HIF-1α, autophagy, and acinar cell survival in LGs.
Growing evidence suggests that the hypoxia-induced activation of HIF-1α, mammalian target of rapamycin (mTOR), and autophagy are integrated, wherein they influence each other and common downstream pathways that affect gene expression, metabolism, and cell survival.[20,21] Autophagy is an evolutionary conserved catabolic pathway that degrades long-lived cellular macromolecules and organelles.[14,20] Following certain stressed conditions, autophagy serves as an alternate cell death mechanism. However, mounting evidence has shown that autophagy can also act as a form of cell survival in which it initiates a cytoprotective pathway to allow the cell to adapt to the stresses induced by starvation and hypoxia.[20] In this study, we found that decreased BVs and subsequent reductions in oxygen content caused HIF-1α stabilization and autophagy activation that protected LGs from cell death. However, in the presence of persistent DE stress, HIF-1α expression decreased and LGs shrunk. These findings were also observed in HIF-1α CKO mice that showed drastically reduced LG size even with short-term DE induction. In humans, LG size decreases with age.[22] This is closely related to lacrimal flow reduction.[23] Therefore, the HIF-1α-induced autophagy system may play a pivotal role in maintaining LG size and flow in the presence of DE.

In addition, BNIP3 expression was elevated in DE-induced LGs. BNIP3 is fully expressed under moderate hypoxia (1–3% oxygen) that can trigger non-apoptotic cell death in mouse embryonic fibroblasts through BNIP3 induction.[24] This pathway is the nonselective autophagy system. However, in severe hypoxia with drastic glucose restrictions, AMPK activation can occur. In this study, DE increased BNIP3 expression without affecting AMPK. Therefore, HIF-1α may activate autophagy through the nonselective system. However, DE also induced increases in ER stress-related enzymes, such as ATG6 and p-PERK, and caused ER dilatations. This suggests that DE may activate the unfolded protein response or ER stress. As AMPK can be activated by ER stress, the activity of AMPK in long-term DE-induced LGs requires further investigation.
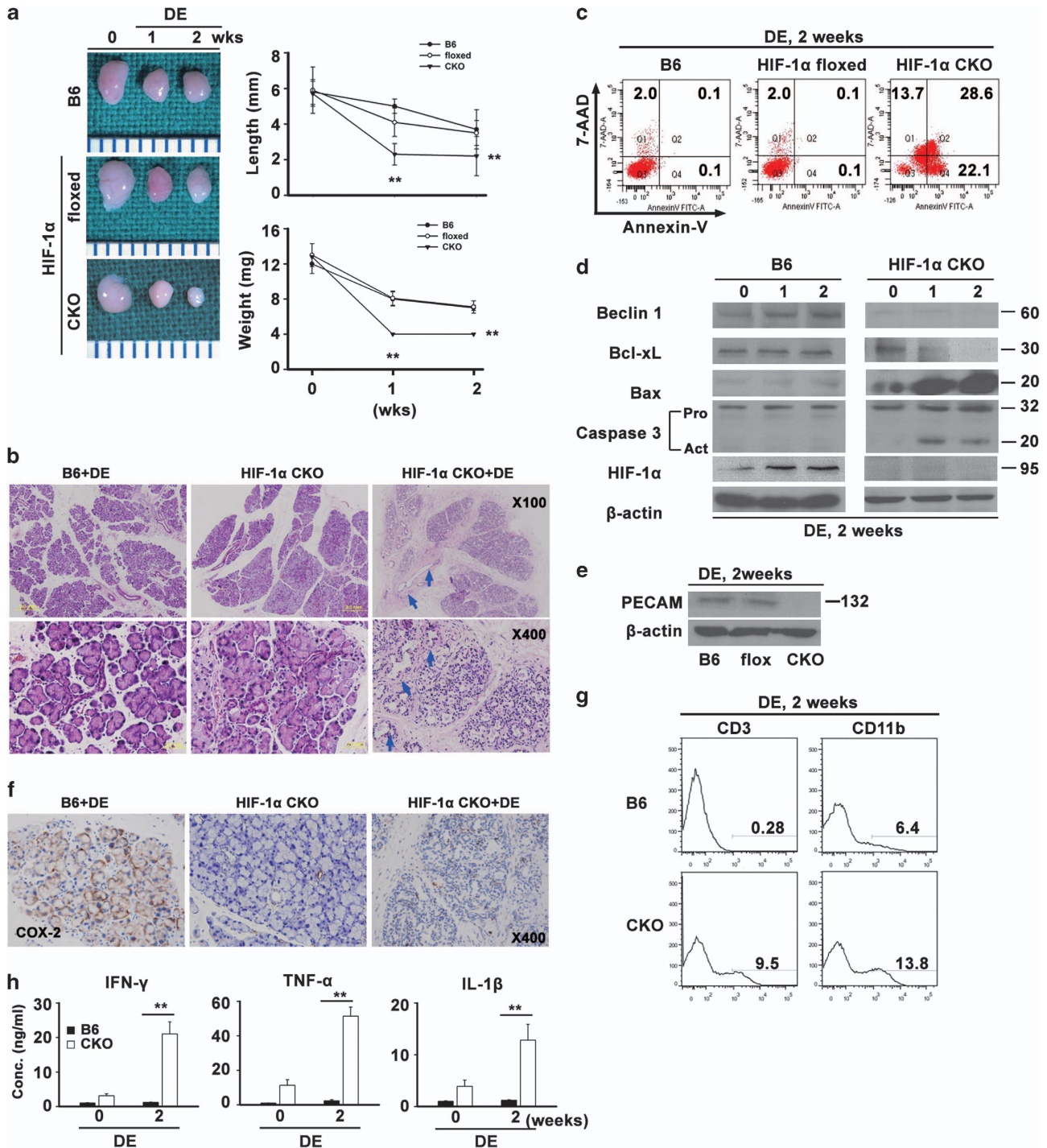
Figure 5 Effect of HIF-1α upregulation on acinar cell death in LGs from DE-induced mice. (**a**) LG size and weight were measured and compared between WT (B6), HIF-1α floxed, and HIF-1a conditional KO (CKO) mice ($n = 6$, **$P < 0.01$, one-way ANOVA). (**b**) Hematoxylin and eosin staining of LGs of HIF-1α CKO mice, DE-induced WT mice, and DE-induced HIF-1α CKO mice. Staining was performed at 2 weeks after DE induction. (**c**) FACS analysis for LG cell death was performed at 2 weeks after DE induction. The preparation of LGs for FACS analysis is mentioned above. (**d**) After DE induction, LGs were secured and prepared for immunoblotting. Anti-HIF-1α (1 : 2000), anti-Beclin 1 (1 : 1000), anti-Bcl-xL (1 : 1000), anti-Bax (1 : 2000), and anti-caspase 3 (1 : 3000) antibodies were used. (**e**) Immunoblotting was performed to detect PECAM (1 : 2000). (**f**) Immunohistochemical staining of COX-2 in LGs of HIF-1α CKO mice, DE-induced WT mice, and DE-induced HIF-1α CKO mice (2 weeks after induction). (**g**) After 2 weeks of DE induction of B6 and CKO mice, the LGs were minced and prepared for FACS analysis of CD11b and CD3. Each cell marker antibody was incubated at 1 : 100 for 1 h. The positive cells were analyzed by FACSCaliber (BD Biosciences). (**h**) Levels of IFN-γ, TNF-α, and IL-1β in the LGs of DE-induced mice were measured by ELISAs. Each conditions included at least six LGs (**$P < 0.01$, Student's *t*-test)

Glucose metabolites are important DAMP signals in DE-induced LGs. We investigated the specific HIF-1α-related DAMP signals in LGs with a focus on glucose metabolites, especially succinate. Succinate continued to accumulate until 2 weeks after DE induction, and isocitrate was significantly depleted. Interestingly, succinate is an endogenous danger signal that stabilizes HIF-1α that consequently regulates the gene expression of IL-1β and other HIF-1α-dependent genes, as well as protein succinylation.[16] Succinate can signal through the G protein-coupled receptor 91 (GPR91) that synergizes with Toll-like receptors and may be activated by inflammatory mediators.[25,26] High succinate concentrations are detected in the plasma of patients with inflammatory diseases.[27] In addition, patients harboring mutations in succinate dehydrogenase demonstrated increased HIF-1α levels.[28,29] Thus, elevated levels of succinate may enhance HIF-1α activation in DE-induced LGs, and this was confirmed using *ex vivo* LG organ culture (Figure 3g). Succinate can also be derived from glutamine through the GABA shunt.[16] Increased levels of GABA were confirmed by LC-MS. This suggests that the depletion of Krebs cycle enzymes and the activation of the GABA shunt may contribute to the accumulation of succinate and other intermediates that then stimulates HIF-1α stabilization and activation.

Pathological changes in HIF-1α CKO LGs. Many HIF-1α-induced cytokines, including VEGFs, IL-1β, and MMPs, are elevated in DE-induced LGs.[8,12,30,31] Nevertheless, the existence, expression, and roles of HIF-1α have not been elucidated in DE-induced LGs. Our findings show that HIF-1α was essential in the prevention of acinar cell death from infiltrating cytotoxic cells and cytokines in the LGs of DE-induced HIF-1α CKO mice.

In this novel mouse model, the majority of glandular structures were lost, and the intralobular and interlobular ducts were dilated and filled with amorphous materials. Interestingly, these changes were quite similar to those observed in the LGs from older DE patients.[32] Furthermore, acinar structures were more severely disrupted in the peripheral areas of LGs than in the central areas. In LGs, the lacrimal arteries divide into branches before entering the glands, and both vascular arcades and interconnected branches are formed.[33,34] Therefore, the peripheral areas of LGs may be less vascularized and more vulnerable to damages that are caused by reduced blood flow. Significant increases in inflammatory cell infiltration were also observed. The mechanism by which cell infiltration was increased in HIF-1α CKO LGs was not determined. HIF-1α is known to mediate COX-2 induction[18,19,35] that can inhibit inflammatory cell infiltration by increasing PGE2 levels. In the LGs of DE-induced HIF-1α CKO mice, the decreases in COX-2 and PGE2 levels may enhance the infiltration of CD3+ and CD11b+ cells. Taken together, these findings may provide an idea for DE treatment strategy. Clinically, the most widely used DE treatment is lubricating the ocular surface, and not the functional regeneration of LG. In our study, HIF-1α CKO mice showed drastic changes such as severe loss of vascularity or cell infiltration even after a short duration of DE exposure. Based on these data, retaining HIF-1α

expression and vascularity of LG could be novel strategies for the DE treatment by preventing further DE-induced damage and by helping recovery of secretary function.

There are several limitations of this study. Our main focus was on the functional role of HIF-1α in DE, and we did not determine the protective mechanisms that were involved in HIF-1α activation/signaling or the neural reflex in the presence of DE. The signaling factors that contributed to the loss of BVs, which was the initial event, remain unclear. In addition, although the DE-induced mouse model is used widely for studying DE, the anatomical location, vascular supply, and pathogenesis of DE are certainly different in humans. It is unknown whether our findings can be directly translated to humans. Human LG studies that utilize radiological imaging are needed.

In conclusion, there are limited studies regarding the nonimmunological mechanisms that are involved in LG damage and protection. Our results demonstrate that HIF-1α played an important role in preventing acinar cell damage from DE stress. Further in-depth studies in mice and humans are needed to understand: (1) the role of neural networks from the ocular surface to LGs in activating HIF-1α, (2) the details of molecular mechanisms in the interaction of HIF-1α and autophagy, and (3) the role of lymphangiogenic activities in DE-induced LGs. In addition, as the pathological changes in the LGs of aged humans[32] are quite similar to that of HIF-1α CKO mice, the DE-induced HIF-1α CKO mouse model can be used to study non-Sjögren's DE disease.

Materials and Methods

Generation of MMTV-Cre-dependent HIF-1α CKO mice. Mice with MMTV-Cre-dependent knockout at the *hif1α* locus were generated by crossing animals containing loxP sites flanking exon 2 of *hif1α* (B6.129-*Hif1α*^*tm3Rsjo*/J; Jackson Laboratory, Bar Harbor, ME, USA). Genotyping was performed using DNA from tail biopsies. Primers for distinguishing floxed from nonfloxed alleles, detecting the MMTV-Cre transgene, and *hif1α* deletion were described in Supplementary 6. All experiments were performed with littermates derived from Hif1αf/f-MMTV-Cre+ × Hif1αf/f-MMTV-Cre− (6–10 weeks old). All procedures in this study were approved by the Animal Care and Use Committee at Yonsei University College of Medicine and conducted according to the Guide for the Care and Use of Laboratory Animals (National Institutes of Health, no. 85-23, 1996).

DE induction and mounting of the eyeball and ocular adnexal tissues. Female C57BL/6 mice (6–8 weeks old, Charles River Laboratory, Wilmington, MA, USA) were used in accordance with the standards of the Association for Research in Vision and Ophthalmology Statement for the Use of Animals in Ophthalmic and Vision Research. Mice were placed in a controlled environmental chamber with <15% humidity to induce DE.[36] To achieve maximum ocular surface dryness, mice received subcutaneous injections of 0.05 ml scopolamine hydrobromide (5 mg/ml; Sigma-Aldrich, St. Louis, MO, USA) once a day for the duration of the experiments. Corneal fluorescein staining score was monitored during the experiments. In addition, TUNEL staining of cornea was performed for verifying the corneal damage more precisely (Supplementary 6).

After DE induction, the mice were killed, and the eyeballs were halved. One half was fixed with 3.7% paraformaldehyde and stored for immunostaining. The other half was stored at −70°C for qPCR.

Immunohistochemical staining of HIF-1α, COX-1, and COX-2. The detailed immunohistochemical staining method has been described previously.[12] The following primary antibodies were used: rat monoclonal anti-mouse COX-1 (Cayman, Ann Arbor, MI, USA), COX-2, HIF-1α, MMP-2, and MMP-9 (Abcam, Cambridge, UK). Antibodies were diluted 1 : 50–1 : 300 and incubated overnight. Sections were observed under a light microscope (Axio Imager 2, Carl Zeiss, Oberkochen, Germany).

For immunofluorescein staining of BVs and LVs, FITC-conjugated anti-PECAM (Santa Cruz Biotechnology, Santa Cruz, CA, USA), anti-LYVE-1 (R&D Systems, Minneapolis, MN, USA), and Cy3-conjugated donkey anti-goat IgG (Jackson Immunoresearch Laboratories, West Grove, PA, USA) were used. The sections were photographed with the Leica DMI6000 B inverted microscope (Wetzlar, Germany) at ×200 magnification and automatically stitched into whole images.

Tissue RNA extraction and qPCR. RNA was isolated using the RNeasy Micro Kit (Qiagen, Valencia, CA, USA) from mouse tissues and reverse-transcribed using the Superscript III Kit (Invitrogen, Carlsbad, CA, USA). Real-time qPCR was performed using the TaqMan Universal PCR Mastermix and preformulated primers for HIF-1α (Mm00468869_m1), COX-1 (Mm04225243_g1), COX-2 (Mm03294838_g1), LDH (Mm00496648_m1), EPO (Mm00438760_m1), VEGF-A (Mm00437304_m1), TNF-α (Mm00443258_m1), IL-1β (Mm00434228_m1), IL-6 (Mm00446190_m1), and GAPDH (Mm99999915_g1) (Applied Biosystems, Carlsbad, CA, USA).

LG size measurement. After DE induction, extraorbital LGs were removed from 12 mice and fixed with 100% methyl alcohol. LGs were vacuum-dried and measured on a scale. Six age- and sex-matched mice were included as controls.

LC-MS analysis for measuring glycolytic activities. Polar metabolites were extracted in 80% methanol. Metabolic profiles were obtained using three LC-MS methods. Two hydrophilic interaction liquid chromatography methods were used to measure polar metabolites in positive and negative ionization MS modes, and one reversed-phase method was used to profile lipids in the positive ion mode. Polar metabolites were profiled in the positive ion MS mode using an LC system comprising 1200 Series Pump (Agilent Technologies, Santa Clara, CA, USA) and an HTS PAL autosampler (Leap Technologies, Carrboro, NC, USA) that was coupled to the 4000 QTRAP mass spectrometer (AB SCIEX, Framingham, MA, USA) equipped with an electrospray ionization source. Sample preparations are described in Supplementary 6.

The MultiQuant software (version 1.2, AB SCIEX) was used to process raw data and integrate chromatographic peaks. The processed data were manually reviewed for quality of integration and compared against known standards to confirm metabolite identities.

Immunoblotting. The detailed immunoblotting methods and antibodies are described in Supplementary 6.

ELISA. At each time point, WT and HIF-1α CKO LGs were collected, lysed, and quantified using the Micro BCA protein assay kit (Pierce, Rockford, IL, USA). IFN-γ (DY485), IL-1β (DY401), and TNF-α (MTA-00b) levels were determined using ELISA kits (R&D Systems).

FACS. FACS analysis was performed as described previously.[30] Briefly, single-cell suspensions of four LGs from each condition were prepared by treating minced tissue fragments with 100 U/ml collagenase D and 15 μg/ml DNase (Sigma-Aldrich) for 40 min at 37 °C. After blocking with 1 μg unlabeled anti-FcrR antibody (clone 2.4G2), cells (1 × 10⁶) were washed with RPMI-1640 and surface-stained with PE-Cy5-conjugated anti-CD11b, PE-conjugated anti-PI (eBioscience, San Diego, CA, USA), FITC-conjugated anti-CD3, PE-conjugated anti-7-AAD (Biolegend, San Diego, CA, USA), or FITC-conjugated anti-Annexin V (eBioscience), and then analyzed by FACS (FACSCalibur, Becton-Dickinson, Mountain View, CA, USA). For the separation of CD45⁺ and CD45⁻ cells in LGs, FACS ARIA (BD) was used after APC-conjugated anti-CD45 staining (eBioscience).

LG organ culture *ex vivo*. LG organ culture was performed as described previously. Briefly, LGs were isolated and washed three times with sterile RPMI solution. Afterwards, they were immersed in organ culture medium, as previously described.[37] LGs were observed for 7 days, with medium changes every 2 days, and immersed in a premixed solution containing succinate, GABA, and lactate (20 μM).

TUNEL staining. LGs were fixed in 10% buffered formalin. Sections (7 μm) were cut, fixed, deparaffinized, and processed using a commercial kit (Oncogene Research Products, Boston, MA, USA) according to the manufacturer's protocol. Sections were analyzed using the Eclipse E600 microscope (Nikon, Tokyo, Japan). Apoptotic cells (dark spots) were counted in 10 random high-power fields.

Statistical analysis. All data are expressed as mean ± S.D. Differences between groups were examined by Student's *t*-test or multivariate analyses using the Newman–Keuls test or ANOVA followed by the Bonferroni procedure for comparison of means using SPSS 18.0 (Chicago, IL, USA). Values of $P < 0.05$ were considered statistically significant.

Conflict of Interest

The authors declare no conflict of interest.

Author contributions

Yuri Seo and Sang Mok Lee designed idea, performed animal experiments, and wrote the manuscript. Yong Woo Ji performed molecular biologic experiments and helped to draft the manuscript. Jongwoo Shim designed idea and performed immunostaining works. Hyemi Noh generated HIF-1α conditional knockout mice, Arum Yeo performed molecular experiments and immunoworks (FACS works). Changhun Park and Min Soo Park helped the analysis of glycolytic metabolites using LC-MS and gave critical interpretation of data. Eun Ju Chang helped design and study conception, and critically revised the manuscript. Hyung Keun Lee designed main idea, wrote, and proved manuscript. All the authors were involved in writing the paper and had final approval of the submitted and published versions.

1. Pflugfelder SC, Solomon A, Stern ME. The diagnosis and management of dry eye: a twenty-five-year review. *Cornea* 2000; **19**: 644–649.
2. Schaumberg DA, Dana R, Buring JE, Sullivan DA. Prevalence of dry eye disease among US men: estimates from the Physicians' Health Studies. *Arch Ophthalmol* 2009; **127**: 763–768.
3. Bron AJ, Foulks GN. The definition and classification of dry eye disease: report of the Definition and Classification Subcommittee of the International Dry Eye WorkShop (2007). *Ocul Surf* 2007; **5**: 75–92.
4. Massingale ML, Li X, Vallabhajosyula M, Chen D, Wei Y, Asbell PA. Analysis of inflammatory cytokines in the tears of dry eye patients. *Cornea* 2009; **28**: 1023–1027.
5. Stern ME, Beuerman RW, Fox RI, Gao J, Mircheff AK, Pflugfelder SC. The pathology of dry eye: the interaction between the ocular surface and lacrimal glands. *Cornea* 1998; **17**: 584–589.
6. Stern ME, Gao J, Siemasko KF, Beuerman RW, Pflugfelder SC. The role of the lacrimal functional unit in the pathophysiology of dry eye. *Exp Eye Res* 2004; **78**: 409–416.
7. Jonsson R, Vogelsang P, Volchenkov R, Espinosa A, Wahren-Herlenius M, Appel S. The complexity of Sjogren's syndrome: novel aspects on pathogenesis. *Immunol Lett* 2011; **141**: 1–9.
8. Hayashi T. Dysfunction of lacrimal and salivary glands in Sjogren's syndrome: nonimmunologic injury in preinflammatory phase and mouse model. *J Biomed Biotechnol* 2011; **2011**: 407031.
9. Zoukhri D. Mechanisms involved in injury and repair of the murine lacrimal gland: role of programmed cell death and mesenchymal stem cells. *Ocul Surf* 2010; **8**: 60–69.
10. Deshmukh US, Ohyama Y, Bagavant H, Guo X, Gaskin F, Fu SM. Inflammatory stimuli accelerate Sjogren's syndrome-like disease in (NZB x NZW)F1 mice. *Arthritis Rheum* 2008; **58**: 1318–1323.
11. Jonsson MV, Delaleu N, Brokstad KA, Berggreen E, Skarstein K. Impaired salivary gland function in NOD mice: association with changes in cytokine profile but not with histopathologic changes in the salivary gland. *Arthritis Rheum* 2006; **54**: 2300–2305.
12. Shim J, Park C, Lee HS, Park MS, Lim HT, Chauhan S et al. Change in prostaglandin expression levels and synthesizing activities in dry eye disease. *Ophthalmology* 2012; **119**: 2211–2219.
13. Crews L, Patrick C, Adame A, Rockenstein E, Masliah E. Modulation of aberrant CDK5 signaling rescues impaired neurogenesis in models of Alzheimer's disease. *Cell Death Dis* 2011; **2**: e120.
14. Hu YL, Jahangiri A, De Lay M, Aghi MK. Hypoxia-induced tumor cell autophagy mediates resistance to anti-angiogenic therapy. *Autophagy* 2012; **8**: 979–981.
15. Tafani M, Schito L, Anwar T, Indelicato M, Sale P, Di Vito M et al. Induction of autophagic cell death by a novel molecule is increased by hypoxia. *Autophagy* 2008; **4**: 1042–1053.
16. Tannahill GM, Curtis AM, Adamik J, Palsson-McDermott EM, McGettrick AF, Goel G et al. Succinate is an inflammatory signal that induces IL-1beta through HIF-1alpha. *Nature* 2013; **496**: 238–242.

17. Takenaga K. Angiogenic signaling aberrantly induced by tumor hypoxia. *Front Biosci* 2011; **16**: 31–48.

18. Jung YJ, Isaacs JS, Lee S, Trepel J, Neckers L. IL-1beta-mediated up-regulation of HIF-1alpha via an NFkappaB/COX-2 pathway identifies HIF-1 as a critical link between inflammation and oncogenesis. *FASEB J* 2003; **17**: 2115–2117.

19. Kim YS, Shin SI, Kang KL, Chung JH, Herr Y, Bae WJ *et al*. Nicotine and lipopolysaccharide stimulate the production of MMPs and prostaglandin E2 by hypoxia-inducible factor-1alpha up-regulation in human periodontal ligament cells. *J Periodontal Res* 2012; **47**: 719–728.

20. Mazure NM, Pouysségur J. Hypoxia-induced autophagy: cell death or cell survival? *Curr Opin Cell Biol* 2010; **22**: 177–180.

21. Wouters BG, Koritzinsky M. Hypoxia signalling through mTOR and the unfolded protein response in cancer. *Nat Rev Cancer* 2008; **8**: 851–864.

22. Ueno H, Ariji E, Izumi M, Uetani M, Hayashi K, Nakamura T. MR imaging of the lacrimal gland. Age-related and gender-dependent changes in size and structure. *Acta Radiol* 1996; **37**: 714–719.

23. Izumi M, Eguchi K, Uetani M, Nakamura H, Takagi Y, Hayashi K *et al*. MR features of the lacrimal gland in Sjogren's syndrome. *AJR Am J Roentgenol* 1998; **170**: 1661–1666.

24. Tracy K, Dibling BC, Spike BT, Knabb JR, Schumacker P, Macleod KF. BNIP3 is an RB/E2F target gene required for hypoxia-induced autophagy. *Mol Cell Biol* 2007; **27**: 6229–6242.

25. Toma I, Kang JJ, Sipos A, Vargas S, Bansal E, Hanner F *et al*. Succinate receptor GPR91 provides a direct link between high glucose levels and renin release in murine and rabbit kidney. *J Clin Invest* 2008; **118**: 2526–2534.

26. Rubic T, Lametschwandtner G, Jost S, Hinteregger S, Kund J, Carballido-Perrig N *et al*. Triggering the succinate receptor GPR91 on dendritic cells enhances immunity. *Nat Immunol* 2008; **9**: 1261–1269.

27. Dahia PL, Ross KN, Wright ME, Hayashida CY, Santagata S, Barontini M *et al*. A HIF1alpha regulatory loop links hypoxia and mitochondrial signals in pheochromocytomas. *PLoS Genet* 2005; **1**: 72–80.

28. Sadagopan N, Li W, Roberds SL, Major T, Preston GM, Yu Y *et al*. Circulating succinate is elevated in rodent models of hypertension and metabolic disease. *Am J Hypertens* 2007; **20**: 1209–1215.

29. Gimenez-Roqueplo AP, Favier J, Rustin P, Mourad JJ, Plouin PF, Corvol P *et al*. The R22X mutation of the SDHD gene in hereditary paraganglioma abolishes the enzymatic activity of complex II in the mitochondrial respiratory chain and activates the hypoxia pathway. *Am J Hum Genet* 2001; **69**: 1186–1197.

30. Ji YW, Byun YJ, Choi W, Jeong E, Kim JS, Noh H *et al*. Neutralization of ocular surface TNF-alpha reduces ocular surface and lacrimal gland inflammation induced by in vivo dry eye. *Invest Ophthalmol Vis Sci* 2013; **54**: 7557–7566.

31. Dartt DA. Neural regulation of lacrimal gland secretory processes: relevance in dry eye diseases. *Prog Retin Eye Res* 2009; **28**: 155–177.

32. Obata H. Anatomy and histopathology of the human lacrimal gland. *Cornea* 2006; **25**(10 Suppl 1): S82–S89.

33. Henker R, Scholz M, Gaffling S, Asano N, Hampel U, Garreis F *et al*. Morphological features of the porcine lacrimal gland and its compatibility for human lacrimal gland xenografting. *PLoS One* 2013; **8**: e74046.

34. Tucker SM, Lambert RW. Vascular anatomy of the lacrimal gland. *Ophthal Plast Reconstr Surg* 1998; **14**: 235–238.

35. Maroni P, Matteucci E, Luzzati A, Perrucchini G, Bendinelli P, Desiderio MA. Nuclear co-localization and functional interaction of COX-2 and HIF-1alpha characterize bone metastasis of human breast carcinoma. *Breast Cancer Res Treat* 2011; **129**: 433–450.

36. Barabino S, Shen L, Chen L, Rashid S, Rolando M, Dana MR. The controlled-environment chamber: a new mouse model of dry eye. *Invest Ophthalmol Vis Sci* 2005; **46**: 2766–2771.

37. Hunt S, Spitznas M, Seifert P, Rauwolf M. Organ culture of human main and accessory lacrimal glands and their secretory behaviour. *Exp Eye Res* 1996; **62**: 541–554.

Supplementary Information accompanies this paper on Cell Death and Disease website (http://www.nature.com/cddis)